High Speed PIV of Breaking Waves on Both Sides of the Air-Water Interface

A.H. Techet, A.K. McDonald

Abstract This paper presents high speed Particle Image Velocimetry (PIV) experiments on small-scale, steep, breaking waves forced by shoaling the waves up an angled slope to a level plateau, in a lidded tank with an initially quiescent air-side. Both spilling and plunging breakers are considered. A PIV system, using a high speed digital video camera at up to 500 frames per second, was used to obtain quantitative data on both the air and water side of the free surface interface. Waves are generated by a computer controlled, paddle-type wave maker at one end of long, narrow acrylic tank. In order to obtain breaking waves on a small scale, surface tension was lowered by mixing isopropyl alcohol with distilled water. Surface tension characteristics of the water-IPA mixture are also presented herein. To perform high speed PIV measurements, a low-cost, Lasiris Magnum, near-IR, TTL diode line generator laser is used to form the light sheet. To seed the water, traditional silver coated hollow-glass spheres were used. While seeding in the water was quite straight-forward, seeding in the air was quite complex. In order not to adversely affect the surface tension, a water-based fog was used to seed the air. Qualitative visualizations and PIV show the formation of the vortex aft of the breaking wave and reveal strong counterclockwise vorticity in the air side of the interface. Results for the plunging breaking wave case are presented herein and compared with numerical results from Hendrickson (2004).

1 Introduction

Wave breaking on the surface of the ocean results in significant transfer of mass, momentum, heat and energy across the air-sea interface. Breaking waves contribute significant dynamic loading to offshore platforms and other offshore structures, and these loads can cause failure due to fatigue or sheer magnitude of the wave force. On a global scale, breaking waves can influence atmospheric and oceanic circulations. Turbulence and bubble entrainment from broken waves enhance the gas transfer from the air to the water in addition to dissipating surface energy. Each of these changes has a direct influence on the circulations which effect global climate; the extent to which wave breaking plays a role in this process is not fully resolved. Understanding the physics of these phenomena remains a challenge, as both the measurement and simulation of the relevant processes are highly complex.

In order to more clearly understand the whole picture, and to generate accurate models of the air-sea exchange processes during wave breaking events, experiments and simulations that consider the physics on both the air and water-side of the air-sea interface are warranted. Recent numerical studies have begun to investigate the air-water coupling during the breaking process, in the absence of ambient wind (*e.g.* Chen *et al.* 1999, Hendrickson 2004), but relatively few experimental studies have looked at flow on both sides of this interface in the absence of wind.

The dynamics of breaking waves have been the subject of many researchers through the decades. Melville (1996) offers an extensive review of the different breaking wave geometries, wave breaking mechanisms, and evolution of the wave profile for deep water waves, and Peregrine (1983) offers a similar review for near-shore breaking waves. Duncan (2001) presents a recent review of existing work in breaking waves, focusing predominately on spilling breakers and highlighting the effect of surface tension on the breaking process. A recent collection of papers discussing research using PIV to study water waves can be found in Grue *et al.* (2004). PIV has been widely used to investigate velocities and turbulence under water waves (*e.g.* Perlin *et al.* 1996, Dabiri and Gharib 1997, Dong *et al.* 1997, Peirson 1997, Melville *et al.* 2002).

A.H. Techet, A.K. McDonald, Center for Ocean Engineering, Department of Mechanical Engineering, Massachusetts Institute of Technology, Cambridge, MA 02139, USA

Correspondence to:
A.H. Techet, MIT Center for Ocean Engineering, Department of Mechanical Engineering, 77 Massachusetts Avenue Room 5-326c, Cambridge, Massachusetts, 02139, E-mail: ahtechet@mit.edu

Breaking waves can be classified as plunging, spilling, surging, or collapsing breakers, though deep water waves include only the spilling and plunging types of breaking. Plunging waves feature the formation of a jet at the crest that projects out from the front face and impacts the free surface with a splash at or below the mean water level. As the front face of the wave overturns, air is entrained and a two-phase turbulent flow ensues beneath the surface. In the more gentle case, spilling breaking waves begin with a small rough zone or bulge forming on the forward tip of the crest. Depending upon the scale, this bulge can include bubbles and droplets or, for smaller scales, a smooth bulge with a train of capillary waves developing beneath it. The turbulent bulge grows by spreading down the front slope and engulfing the face of the wave. Surging and collapsing waves occur at the shoreline and are closely related. Reflections are significant in these shallow water events. In surging breaking, there is no significant disturbance in the wave profile except at the moving shoreline. The collapsing wave combines characteristics of both surging and plunging breakers, whereby a plunging jet forms on the lower portion of the face of an otherwise surging wave. Neither collapsing nor surging waves were examined in this study.

In addition to their geometry and kinematics, breaking waves are classified by their temporal evolution as steady, unsteady, or quasi-steady. Unsteady breaking waves are the most commonly occurring class of breakers in the open ocean and near the shoreline. The breaking event is brief, typically ending within a wave period, though turbulence may still persist in the flow. Once the excess energy that led to the breaking event has dissipated, the breaking expires. The attributes which expire in the unsteady case are sustained over time in steady breaking. Steady flow over fixed objects or flow over objects in tow can result in steady wave breaking, and the breaking continues to dissipate energy as long as the input energy source is maintained (*e.g.* Duncan 1981, Dabiri and Gharib 1997). Quasi-steady waves always take the form of a spilling breaker. However, the turbulent bulge near the crest does not propagate down the front face of the wave as it does in the unsteady spilling breaker. The wave off a ship in transit is characterized as quasi-steady, though it often has a plunging component.

The methods for inducing wave breaking in the numerical realm are comparable to those used in experimental techniques. Comparisons of simulations with experimental data are highly useful for modeling the physical processes in breaking events as well as validation. Dommermuth *et al.* (1988) present a comparison of potential theory simulations and experiments for deep-water plunging breakers. Refinements in the original numerical schemes and increased computer processing capability have improved the methods through inclusion of more physical effects. Recent advancements have yielded simulations which include parameters such as viscosity, surface tension, and the air-effects, but they have also been limited to very small scales.

Several numerical approaches have been used to examine the turbulence and fluid structures that develop over the entire breaking process, on both the air and water side of the free surface. For example, Chen *et al.* (1999) overcome the potential flow limitations by using a two-dimensional volume-of-fluid (VOF) method to create viscous plunging waves in a liquid-gas medium. In the VOF approach, two different phases are approximated by the flow of a single fluid whose physical properties, such as density and viscosity, change across the interface. Chen *et al.* implement a direct numerical simulation of the Navier-Stokes equations and compute the motion of a gas and liquid through jet impact and splash-up. Although the properties used in the simulation were not equivalent to air and water (the ratio of fluid densities was $\overline{\rho} = 10^{-2}$ and the ratio of fluid viscosities was $\overline{\mu} = 0.4$) the results appear qualitatively similar to a short wavelength plunging breaker.

Iafrati *et al.* (2001) use a Navier-Stokes solver with a level set method to simulate a plunging wave resulting from flow over a bump. They use the properties of air and water and establish qualitative agreement with the experimental observations of Bonmarin (1989). Though the results from VOF and level set method simulations have not been quantitatively verified through experiments, they mark a distinct improvement over potential theory in that they can incorporate viscosity and turbulence as well as the dynamics of flow on the air-side of the interface.

More recently, Hendrickson (2004) looked at breaking waves with a Direct Numerical Simulation of the Navier-Stokes equations using a modified level set method. At the air-water boundary, the traditional level set method is subject to shear discontinuities due to large velocity gradients near the surface of the air-side. To resolve the shear errors, Hendrickson implements an asymmetric smoothing function which extends the level set boundary layer on the air-side only. Having tested and analyzed the resulting modified level set, Hendrickson uses the improved method to generate a deep-water wave breaking database. Quantitative data obtained through PIV, on a scale comparable to Hendrickson's simulations, can be used to validate the numerical results and advance modeling efforts up to real-world scales.

This paper presents high-speed PIV experiments on small-scale, steep waves forced to break by shoaling the waves up a fifteen degree slope to a level plateau. Waves are generated by a computer controlled, paddle-type wave maker at one end of small acrylic tank. The waves generated in this tank were smaller in scale than in typical wave

breaking experiments, in order to compare with numerical simulations by Hendrickson which were on the order of Reynolds number 10^3-10^4. Achieving breaking in the tank at these scales required a lower surface tension than possible with pure distilled water. Thus isopropyl alcohol (IPA) was mixed with the distilled water to reduce the surface tension. Attempts to quantify the flow of the air side of the wave, in the absence of wind, are performed using a water-based fog as air-side seeding. Results from high speed PIV and qualitative flow visualization experiments are presented in §3 for both the air and water side of the free-surface interface.

2 Experimental Setup

Small-scale spilling and plunging microbreakers are generated in a clear acrylic wave tank. Particle Image Velocimetry (PIV) and qualitative visualization are used, with high speed video acquisition, to observe the flow features on both sides of the air-water interface. To help characterize the waves, Reynolds number and Weber number are calculated and presented for the upstream wave formed by the wave paddle and yet unaltered by the sloping shoal. To define the wave characteristics both Reynolds number and Weber number are calculated, along with upstream phase speed, *Cp*, and wave slope parameter, *ka*, where *k* is the wavenumber. Reynolds number is defined as

$$Re = \frac{\rho U \lambda}{\mu}, \tag{1}$$

where ρ and μ are the fluid density and viscosity, and U and λ are the phase speed and wavelength of the associated wave. The waves in this study are smaller than those typically examined in other experimental research efforts in order to facilitate comparisons with ongoing numerical studies by Hendrickson (2004). Numerical simulations by Hendrickson (2004) were on the order of Reynolds number 10^3-10^4, and the Reynolds numbers for the experiments discussed herein were between $9x10^4$ and $2x10^6$. Since these waves are small in scale, surface tension plays a large role and must be quantified. Weber number is used to characterize surface tension and is defined as

$$We = \frac{\rho U^2 \lambda}{\sigma}, \tag{2}$$

and σ is the value of surface tension at the fluid surface. Weber numbers for the experiments presented in this paper range from 2.3×10^3 to 9.8×10^4. A discussion of the effect of surface tension on spilling breakers can be found in Duncan and Liu (2003).

Experiments were performed in a small acrylic tank with inner dimensions of 2.5 *m* in length, 16 *cm* in width and 18 *cm* in height (see Figure 1). A piston-driven, pivoted wave paddle at one end creates precise, small-scale waves that propagate down the tank, while an energy absorbing beach mitigates reflections at the opposite end. The wavemaker is driven by a servo-controlled, moving coil, linear actuator, which has an encoder resolution of 5 *microns*, a 5 *cm* stroke length, and a maximum load capacity of 2.5 *lbs*. A PC and external motion controller provide closed loop control for the wavemaker during actuation. An energy absorbing beach was constructed at the far end of the tank. The beach was designed to absorb maximum wave energy with materials that would not leach into the water.

Wave breaking was induced by propagating a monochromatic wave train over a constant slope section to a level plateau. In this shoaling method, the wave energy is focused into a smaller volume until breaking occurs. Since bottom effects become significant, these waves are fundamentally different from the deep water breaking waves often presented in literature. However, the free surface geometries of the resulting breakers are similar to the deep water cases, and the breaking types are thus characterized using the same terminology (*e.g.* spilling, plunging, surging). The shoal section used to induce wave breaking in this study is similar to that used by Tsai *et al.* (2005).

The waves were induced to break by propagation up a 15° slope to a level plateau. This angle of 15°, or 1/(3.73), is considered to be quite steep. The fifteen degree slope was chosen for further study here because it resulted in the most energetic breaking, and was found to creating the larges range of plunging breakers in the small tank. The sloping shoal transitions to a flat plateau at a height of 10.2 *cm* above the tank floor, the depth of the water on top of the plateau was varied with the overall water depth in the tank. The free surface displacement in time was measured using a set of three resistance-type, surface piercing wave gauges designed for freshwater. Two probes were placed well upstream of the breaking region and one probe was placed downstream of the shoaling region.

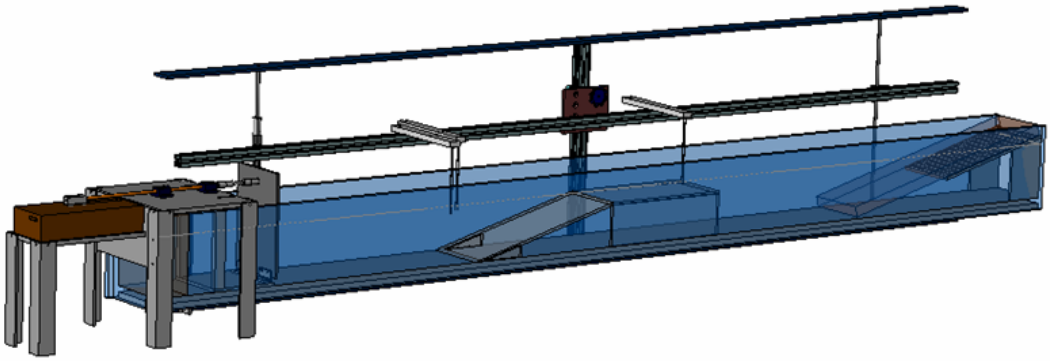

Figure 1 SolidWorks view of the tank, wavemaker, and wave gauge mounting rack. The energy absorbing beach and shoal section are also shown.

Since the waves generated in these experiments are small in wavelength, surface tension at the air-water interface was an important factor affecting the breaking process. For reference, Duncan (2001) describes the effects of surface tension in his review of spilling breakers. Preliminary results from the breaking waves in this study did not feature the formation of a plunging jet for any case when performed in filtered tap water, with surface tension at 74 *dynes/cm*. In order to reduce the surface tension, isopropyl alcohol (IPA) and distilled water were mixed, and the ratio was varied to observe changes in wave breaking dynamics. Isopropyl alcohol was added because of its low surface tension (22 *dynes/cm*) and complete miscibility in water at all concentrations. IPA also forms azeotropic mixtures with water, so there should be no change in the concentration due to evaporation of the mix. Surface tension was characterized by the Wilhelmy plate technique over a range of IPA and water solutions. Quantifying surface tension through experiments was critical in this research because the surface free energy can dramatically effect wave deformation during breaking.

Control experiments were performed to determine the effect of concentration of IPA in water on surface tension. The Wilhelmy Plate method was used to measure the static surface tension in 100mL sample volumes of various IPA concentrations. These results were compared to data published in the semiconductor industry, where IPA is used for Marangoni wafer drying (see Kittle 2002). Results obtained in our tests matched the published data with excellent agreement (see Figure 2(a)). Tests were also performed on 10% and 20% concentrations of IPA, as well as on mixes in the presence of fog particles and PIV particles. Since plunging waves could be produced in the 3% non-mixed solution, well-mixed concentrations higher than 20% were not expected to be required for forming jets. A plot of the complete results is illustrated in Figure 2(b). Neither the PIV particles nor the fog particles change the surface tension significantly, and surface tension did not appear to vary significantly in time, on the order of the time taken to perform each experiment.

Before filling the wave tank for testing, care was taken to ensure that the conditions of the tank reflected those of the isolated experiments. The inner walls were cleaned with pure IPA to remove any contaminants. Gloves were worn to prevent hand oils from contaminating the fluid and affecting surface tension. The tank was also covered to contain the fog during PIV and to prevent airborne particulates from contaminating the surface. Additionally, a polycarbonate plate was used to skim the surface before testing.

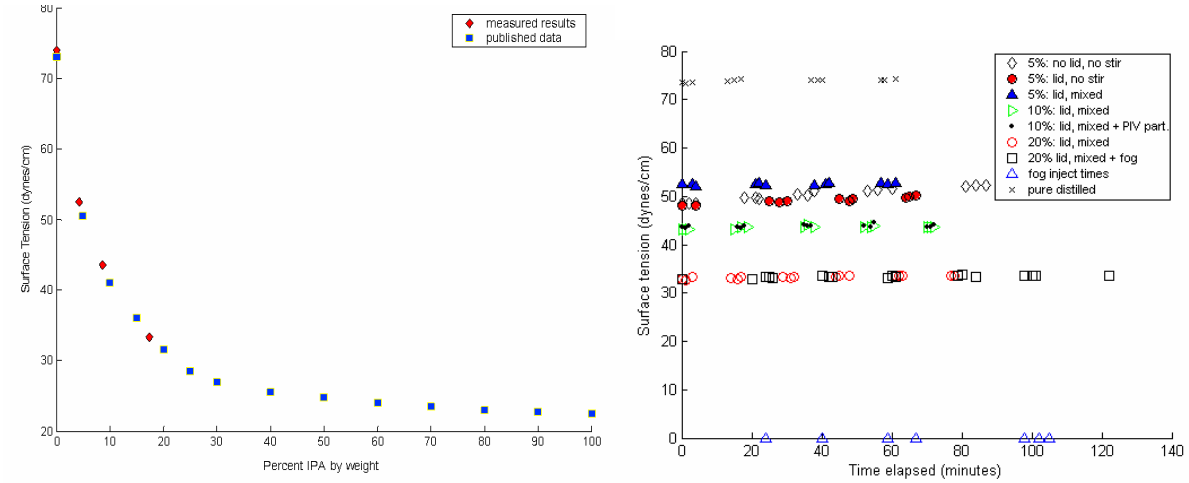

a. b.

Figure 2 (a) Plot of the change in surface tension versus the percentage of IPA (by weight) in distilled water. The measured results are plotted alongside data published in Kittle (2002). (b) Surface tension measurement results for three different IPA concentrations with and without fog and/or PIV particles.

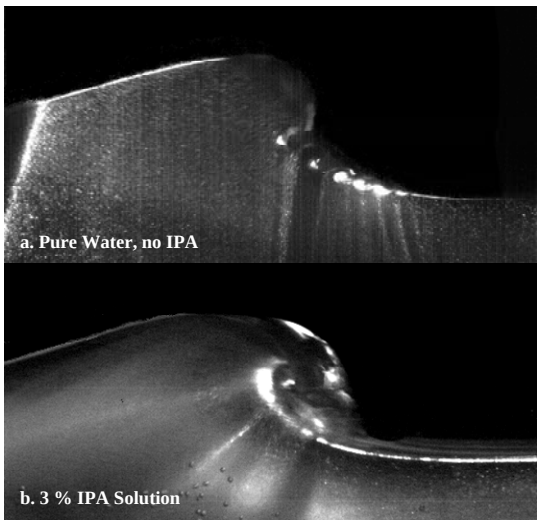

Figure 3 Effects of IPA on a 2Hz ($\lambda \approx 40$ cm) breaking wave with 2.25 cm input amplitude. (a) Spilling wave generated with distilled water with PIV particles. (b) A characteristic plunging breaker forms in a solution of 3% (by volume) of IPA in distilled water with PIV particles.

The effect of adding IPA to water can be seen in the images of waves shoaling up the slope seen in Figure 3. Figure 3(a) shows the spilling wave generated by a wave train with frequency of 2 *Hz* and characteristic wavelength λ = 40 *cm*, with pure, distilled water, and figure 3(b) shows the plunging breaker generated by the same wave train as the wave in figure 3(a) but with a 3% solution of IPA mixed in water. The breaking waves presented in the subsequent sections were made by varying frequency and amplitude of the wave paddle in a 10% IPA solution.

High speed particle image velocimetry (HS PIV) was used to obtain quantitative data above and below the air-water interface. A review of the last 20 years of PIV can be found in Adrian (2005), and an excellent treatment of the technical details of the PIV method is found in the book by Kompenhans *et al*. (1998). The system used for these experiments was built in an *ad-hoc* fashion using an IDT XS-3 high speed video camera (1260x1024 pixels at 628 frames per second maximum), synched with a Lasiris brand Magnum laser, to illuminate the flow. The diode laser operated in the near-IR range (810 nm wavelength) and emitted a single sheet of light with a 20° fan angle. The maximum laser power output was 3.6 Watts. The laser operated on a 12V power supply, drawing a maximum 6.0 amps. The laser sheet was aligned vertically in the direction of wave propagation and could be positioned above or below the tank. The camera imaged through the side of the tank.

While seeding in the water was quite straight-forward, seeding in the air was quite complex. The seeding material used in the water was standard 14μm diameter, silver-coated, hollow glass spheres from Potters Industries. Although the tank was lidded, the air side was a challenge to seed. Air-seeding techniques such as atomized oil droplets are not appropriate in this study as the oil would negatively influence the surface tension and make it hard to obtain plunging breakers. Thus a water-based fog was used to seed the air. Luckily, no change in surface tension was recorded by addition of the fog. It is good to note, also, that the standard particle seeding in the water did not have significant effect on the surface tension measurements once the particles were well mixed and any excess was skimmed from the free surface. Unfortunately the fog based air seeding was not an ideal flow tracer, as the fog was quite dense and it was hard to visualize the plane located mid-tank that was illuminated by the light sheet. In addition the fog particles were too small in comparison to the water-side seeding. However, qualitative images and preliminary PIV data shows good qualitative agreement with numerical simulations by Hendrickson (2004).

Particle images were recorded with the IDT camera at 500 Hz in a modified field of view with 1260H x 404V pixels. Particle images were processed using the LaVision DaVis software package with multi-pass, time-series cross-correlation, a final window size of 16 x 16 pixels and a median filter used to remove spurious vectors. Vorticity was calculated from the velocity fields, and the resulting plots show regions of clockwise vorticity in red, regions of counter clockwise vorticity in blue, and zero vorticity in green. A review of the performance of the LaVision DaVis PIV software package is presented with the results of the Second International PIV Challenge at PIV03 (Sanislas *et al.*, 2005). In addition to using the images for PIV post-processing, the recorded video was used to create profiles of the 2D wave deformation during breaking, on the plane illuminated by the laser (figure 4). To determine the surface profile a Sobel edge detection algorithm from the Image Processing toolbox in MATLAB was used on the PIV images.

3 Results

The typical characteristics of a small scale spilling wave, similar to those described by Duncan (2001), are illustrated in the surface profiles plotted in Figure 4(a). The image displays four superimposed wave profiles captured at distinct intervals throughout the breaking process. The spilling event was generated by a 3Hz wave, with an upstream amplitude of 0.7 *cm* and wave slope $ka = 0.233$. The profiles were generated using a Sobel edge-finding method which is included in the MATLAB Image Processing Toolbox. This edge-finding algorithm was applied to the spilling images obtained using the high speed camera, laser sheet and seeded solution. Note that the wave profile becomes steeper at the top of the slope and forms a bulge-toe shape at the crest. The toe spills then down the face of the wave under the influence of gravity and forms a turbulent region. The turbulence engulfs the front face of the wave just as it moves beyond the illuminated region. While the laser sheet illuminated a two-dimensional section of the flow, three-dimensional effects made it difficult to resolve the edge with high precision. Thus, some edges were more blurry. The bulge, toe and capillary wave system were apparent in all test runs, with a more pronounced bulge forming for the steepest waves of large amplitude. Since Hendrickson's simulations scaled surface tension effects to create gentle spilling through plunging breaking waves, an analogous experimental technique was employed to reduce the influence of surface tension on the waves in this study.

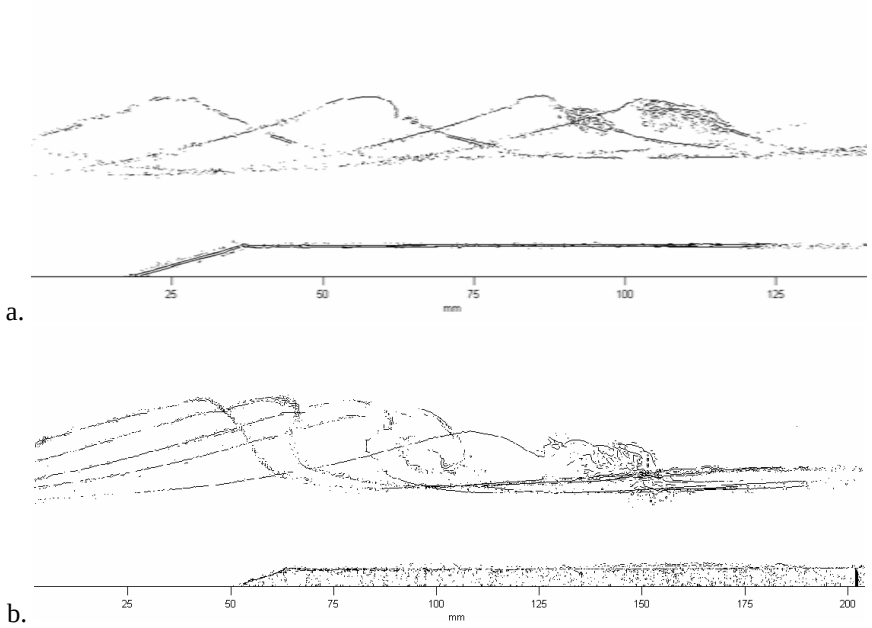

Figure 4 Wave profile determined using MATLAB edge detection routine for (a) spilling breaking wave (3Hz upstream) and (b) plunging breaker (2 Hz upstream).

The use of isopropyl alcohol mixed into distilled water changed the surface tension such that a plunging breaker could be created. The profile of a typical plunging breaking wave is illustrated in Figure 4(b), featuring a pronounced jet forming as the face of the wave becomes vertical. The plunging breaker was generated by a 2 *Hz* incoming wave, with upstream amplitude of 1.08 *cm* and wave slope $ka = 0.186$. This wave was the most dramatic plunging wave that the system could generate.

Figure 5 (a) shows a sequence of images obtained with high speed video for the plunging case from Figure 4(b). Five frames from the high speed video illustrate the sequence of wave breaking. The camera was positioned at a slight angle to highlight any three-dimensional breaking effects. The images clearly show three-dimensional effects, as the waves appear to break differently at the wall than in the middle. In the plunging case, for example, the jet and air entrainment were much more pronounced at the center of the wave. Transverse waves were also present in the tank and appeared as smaller ripples on the primary wave train.

Wave elevation upstream and downstream of the breaking region was recorded from the wave probes. The wave data was also used to provide information needed to calculate the Reynolds and Weber numbers and to give insight into the potential energy lost to breaking. Two closely spaced probes at the start of the ramp were used to determine the phase speed, C_p, of the wave train before shoaling. The wavelength was found by dividing the phase speed by the wave frequency. The third, downstream probe measured the amplitude of the wave train after the breaking event. The energy dissipated during the breaking event was estimated using the difference between the square of the amplitude upstream and downstream of the slope. Although these waves are non-linear, this calculation provides a rough, first order estimate of energy dissipation which has been used by researchers such as Rapp and Mellville (1990) and Hendrickson (2004). For the plunging case presented herein, the remaining energy after the breaking event was approximately 4.5% of the upstream available energy.

A plot of the potential energy loss across all cases is shown in Figure 6. The general trend is that waves with higher initial slopes lose more energy to breaking and reflections when they encounter the shoal. With the exception of the 2Hz plot, there is a significant jump in energy loss between the non-breaking and spilling cases. The hollow shapes, representing cases where the wave breaks prematurely off the wave paddle, do not generally follow the trend, most likely due to the complexity of upstream breaking off the paddle causing early turbulent losses. In all cases of breaking off the paddle, waves dissipated more energy between the probes than others of the same input frequency.

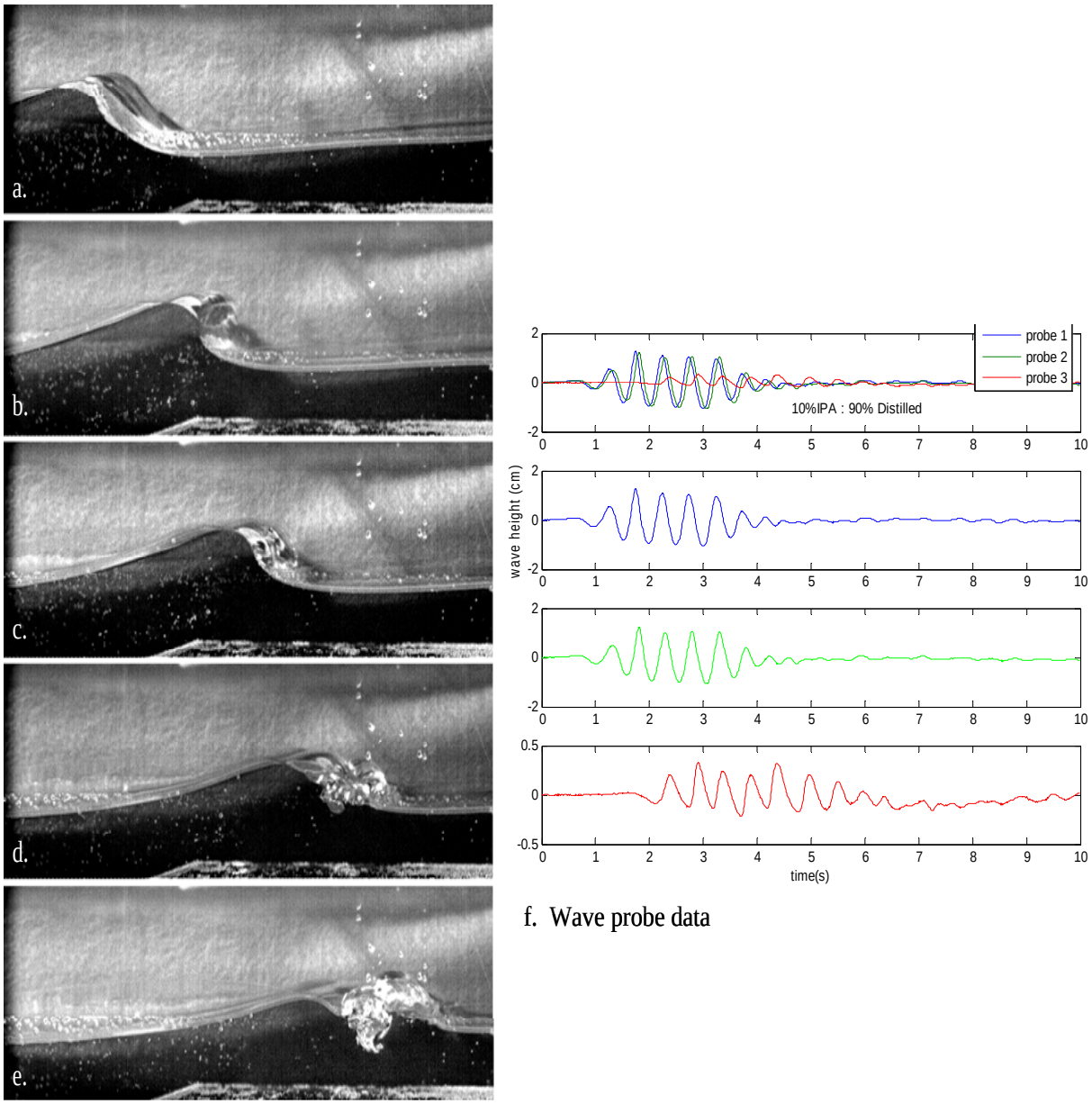

f. Wave probe data

Figure 5 Image sequence for a plunging breaker (a-e) and probe data (f) obtained for wave with kinematic parameters corresponding to the 2.0 *Hz* frequency case generated in five wave paddle cycles. The paddle amplitude was 2.25 *cm*, upstream wave amplitude *a* = 1.08 *cm*, wave slope *ka* = 0.186 (λ = 36.6 *cm*) and phase speed *Cp* = 0.73 *m/s*.

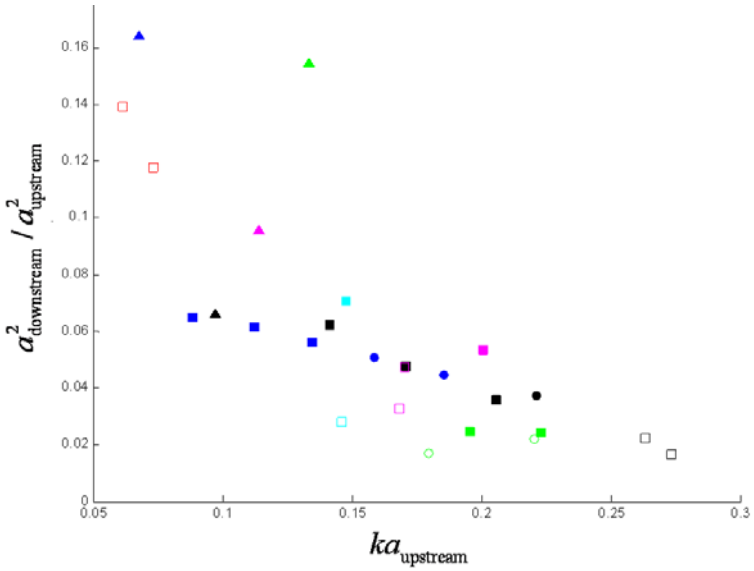

Figure 6 Plot of fractional remaining potential energy for all cases in the wave breaking database. The shape of the points (circle, square, triangle) indicates the type of breaking (plunging, spilling, non-breaking). The hollow shapes indicate cases of premature upstream breaking or shoal vibration. The colors represent the frequency of the wavetrain: red = 1.5Hz, blue = 2Hz, black = 2.5Hz, green = 3Hz, magenta = 3.5Hz, cyan = 4.0Hz.

Note in figure 6 that the slope parameter on the x-axis is slightly misleading, as the data was recorded before the waves encountered the shoal. The sloping bottom concentrates the wave energy and the waves get steeper as they propagate over it. Thus, the slopes associated with the different types of breaking are well below the Stokes limiting height. They should not be interpreted as slopes at the onset of breaking or to establish a breaking criterion.

The 2Hz waves were most ideal for the current experimental set-up. The full range of waves from plunging to spilling to non-breaking was realized by lowering the input amplitude from the maximum 2.5cm. The plot shows that the waves with the highest upstream slope lose the most potential energy. The transition from plunging to spilling occurs at a slope between 0.135 and 0.159. The remaining energy appears linear with slope through all the breaking cases with a sharp increase in the non-breaking case. Interestingly, the change in energy remaining between the most violent plunging and spilling waves is only 2%. This could be due to a wave interaction with the shallow plateau section between the top of the slope and the downstream wave probe. If these experiments were performed in deep water, the plunging jet would transmit energy deeper into the water column and dissipate energy faster. The results from the plot of potential energy losses due to breaking agree with expectations, at least qualitatively. These measurements are also subject to error of the wave probes (8-10% error).

PIV was performed on both spilling and plunging wave cases. Only data from one plunging case is presented herein. Further PIV datasets can be found in McDonald (2005). Figure 7 shows PIV results for the plunging wave generated from a 2.0 Hz wave with upstream amplitude of a = 1.08 *cm*, slope parameter ka = 0.186 and phase speed Cp = 0.73 *m/s*. In this case the plunging jet entrains air and causes a significant splash-up. The dotted line indicates where the source of the splash-up originates from (either the jet or the trough fluid). A mixed gas-liquid flow develops in the turbulent region under the breaker.

The velocity fields in Figure 7 show that the highest particle velocities (red arrows) are near the crest, as expected. The arrows trace paths which converge at the crest where the jet develops. As wave slope transitions beyond vertical, the plunging jet shadows some of the wave from the laser light, preventing it from being resolved well. The maximum velocity appears in frame 2, as the wave ejects and the jet falls under gravity. In frame 3, the jet has just impacted the surface, causing the splash-up phenomenon described in Bonmarin (1989). It appears as though the upper region of the splash up is made of particles from the reflected jet, while the underside is composed primarily of fluid from the trough. As plunging motion continues, the entrained air and water undergo turbulent mixing. Unfortunately, the turbulent region is not fully resolved spatially and warrants further investigation.

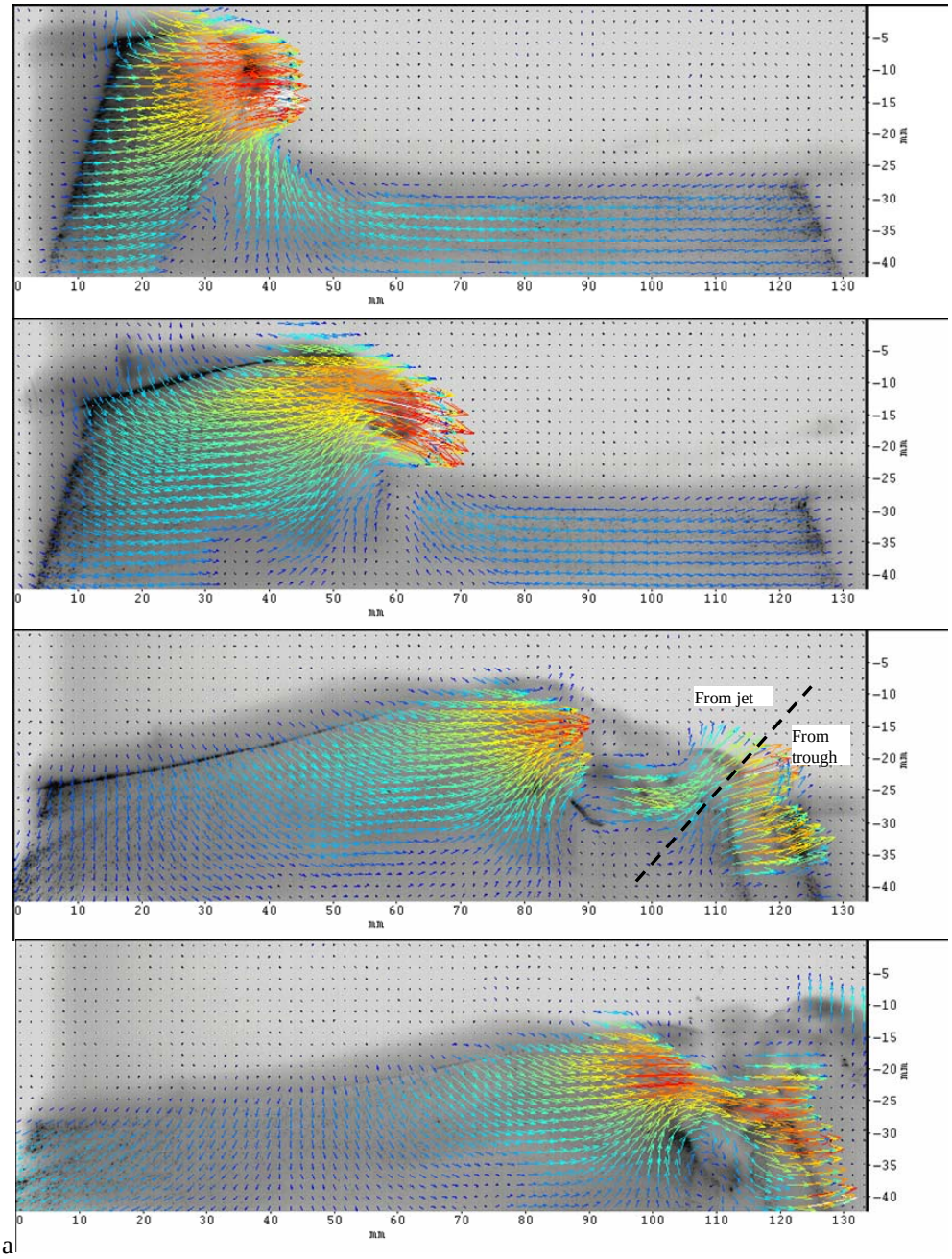

a

Figure 7 Velocity field for the plunging wave generated from a 2.0 Hz wave with upstream amplitude of *a* = 1.08 *cm*, slope parameter *ka* = 0.186 and phase speed *Cp* = 0.73 m/s. The plunging jet entrains air and causes a significant slash-up. The dotted line divides source the splash-up. A mixed gas-liquid flow develops.

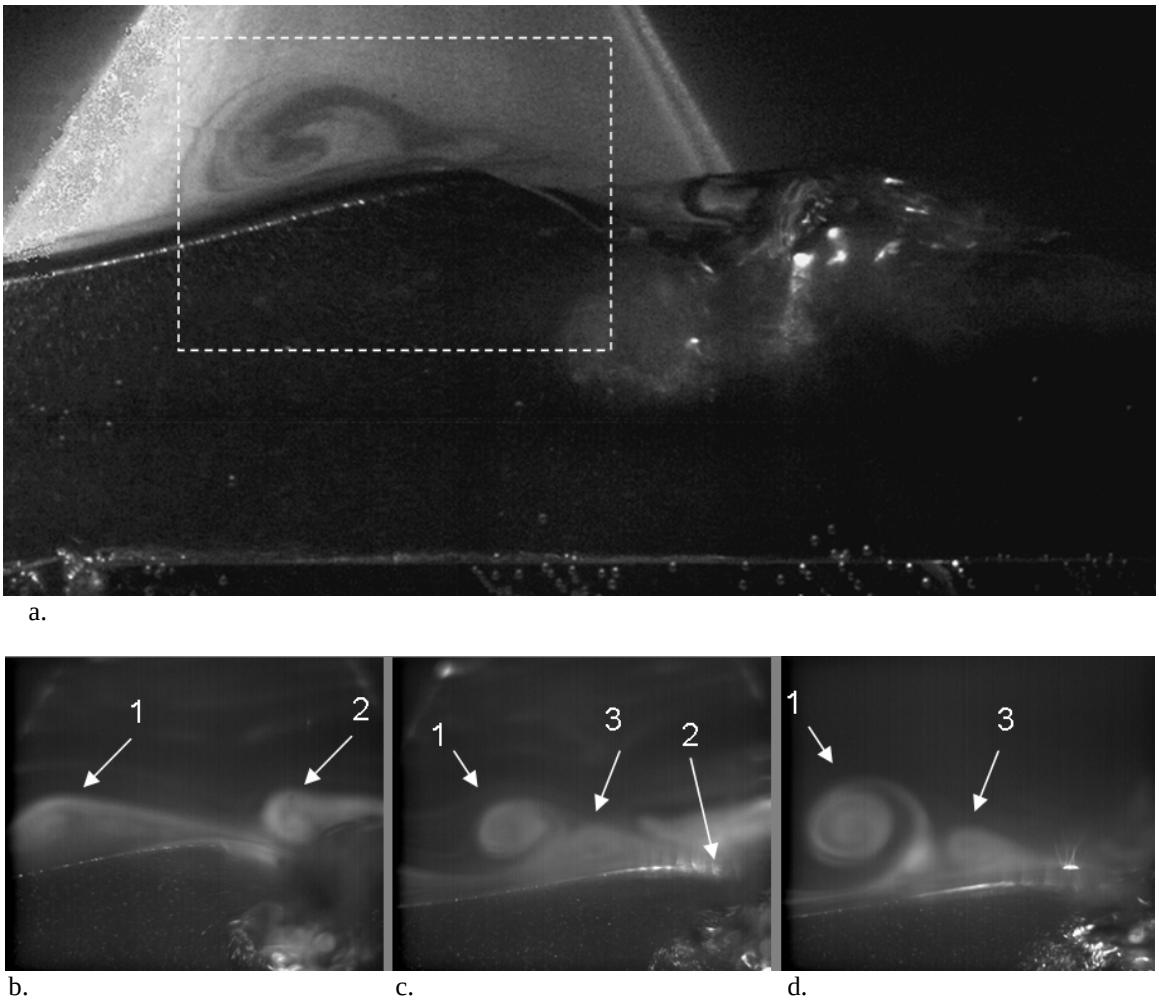

Figure 8 Qualitative visualization of the vortex shed off the back of a plunging breaker. (a) A wide angle view of a vortex in the air above a plunging breaker, after the plunging jet has impacted the water and caused splash-up. (b-d) Close-up of the vortices developing in the air after the plunging jet has impacted the water and caused splash-up. The evolution of smaller vortices can be seen in temporal progression from left to right and the individual vortices are labeled.

Air flow structures above the breaking wave were visualized by injecting fog into the lidded tank. The same plunging wave discussed above was examined in these tests, with Reynolds and Weber numbers around 280,000 and 5200, respectively. The high speed video, recorded in dense fog seeding conditions, displays air-side vortices developing at the back of the wave after it plunges. One large primary vortex appears in Figure 8(a) which revolves counter-clockwise. This feature is comparable to the vortex shed in the classic problem of flow over a hill. In this case, it expands and moves upward as the broken wave propagates forward. Figure 8(b-d) shows a close-up view of the boxed region in image (a) as the flow evolves in time. Image (a) occurs at a later time that (b-d). A closer look at the sequence (b-d) reveals the formation of smaller vortices near the primary vortex.

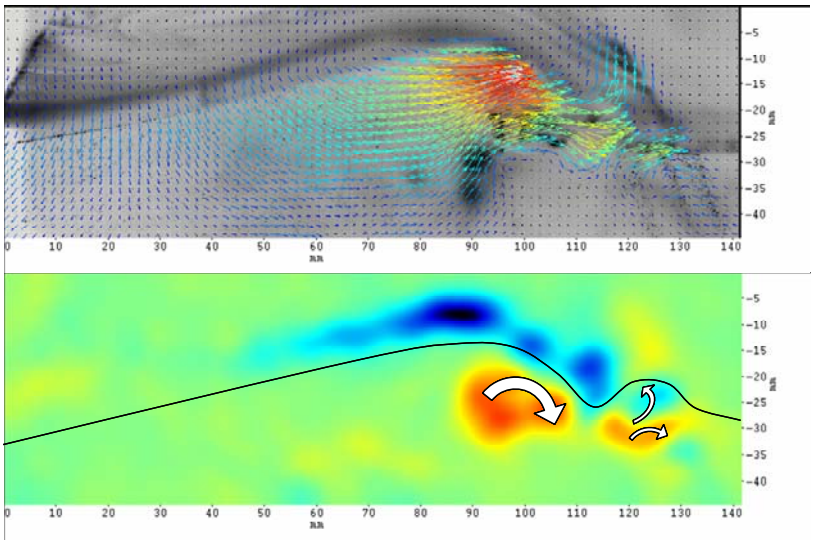

Figure 9 Splash-up event after the plunging jet impacts on the free surface. PIV velocity field (top) and vorticity (bottom) are shown. Red vectors indicate high velocity and blue vectors indicates lower velocity. Red vorticity, as indicated by the superimposed arrows, is clockwise, and blue vorticity is counterclockwise.

Bonmarin (1989) discussed the structures present after the jet has impacted the water through the splash-up and flow degeneration. In addition to the pocket of air entrained as the jet impacts the surface, he describes a process where air entrainment occurs due to the interaction of the plunging jet with the rear vortex of the splash-up. This process is evident in figure 8(c), where vortex "2" is consumed in the fluid wedge. As vortex "1" moves upward from the free surface, a third vortex appears which also rotates in the counter-clockwise direction. PIV details of the splash-up region, similar to that described by Bonmarin, in conjunction with air-side PIV (with every two vectors shown for easier viewing), appear in figure 9. In the lower image of the vorticity, the wave profile and splash-up directional arrows were added to indicate the sign of the vorticity.

Difficulties associated with achieving uniform fog seeding made resolution of the air flow less than ideal for PIV. The fog particles were much smaller than the particle tracers in the water making simultaneous measurement challenging. In addition, only a single laser was used and regardless of whether it was mounted shining up or down, there was significant refraction of the light through the free surface making it difficult to measure both sides of the flow simultaneously. Various processing techniques were used to obtain better resolution of the velocity field on the air side in cases where the seeding was less dense than in figure 8. Overall, the velocity fields primarily map large scale motions rather than the smaller scale features. However, the processed velocity and vorticity fields in the mixed seeding case do yield very similar results on the water side of the free-surface, when compared to the case without fog seeding in the air.

4 Concluding Remarks

PIV and qualitative visualization was performed for small-scale breaking waves. Water-side PIV was performed using traditional seeding methods, whereas air-side measurements were attempted using a water-based fog. Vorticity results of the combined visualizations reveal qualitatively similar results to numerical studies by Hendrickson (2004). Figure 10 compares the vorticity data obtained for the 2 Hz plunging breaker with Hendrickson's numerical simulations. Blue vorticity indicates counter-clockwise rotation and red clockwise rotation.

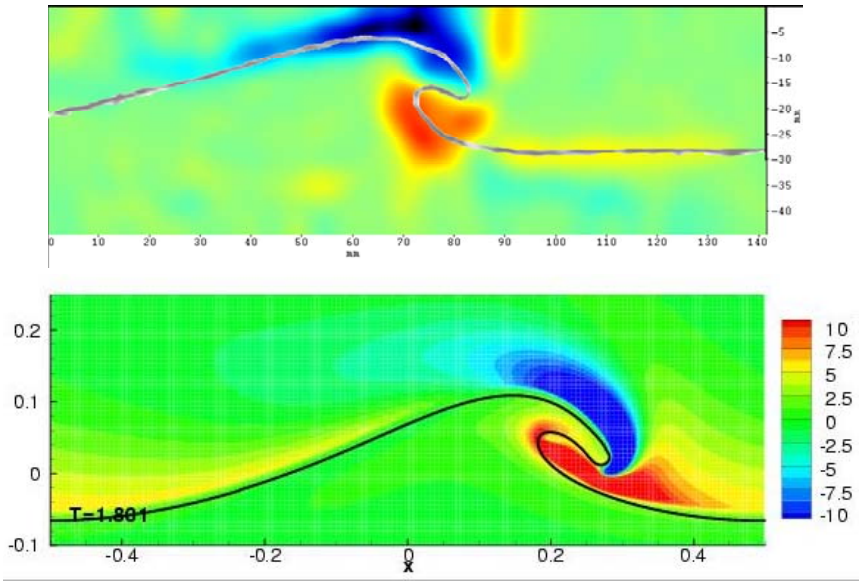

Figure 10 Qualitative comparisons of experimental PIV data (top) with level set numerical simulations (bottom) by Hendrickson (2004). Blue vorticity indicates counter-clockwise rotation and red clockwise rotation. Green represents zero vorticity. The vorticity color maps in the two images are not identical.

Using direct simulation of the Navier-Stokes equations, Hendrickson computes a plunging wave profile using an impulsively started Airy wave. The Reynolds number for her simulation was 2,000 and the Weber number was set at 73,868 to reduce the influence of surface tension. Though the breaking mechanism and scaling parameters were different than in Hendrickson's study (experimental tests were performed at Reynolds and Weber numbers around 280,000 and 5200, respectively), the resulting vorticity plots and profiles are similar. It should be noted that, in the experimental data, the tip of the plunging jet, and the region of air beneath it, were not clearly visible in the video, making it difficult to resolve the flow field in this region. Hendrickson's simulation shows more clockwise (red) vorticity in the air, which may actually exist but was not captured in experiments. The counterclockwise (blue) vorticity on the back of the plunging wave is similar to region in the numerical model, as expected from the qualitative visualizations in figure 8. The region of clockwise (red) vorticity in the experimental results extends further and deeper into the fluid than in the simulated result. This discrepancy could be a result of bottom interaction with the shoal and plateau or the processing techniques.

Significant improvements to the air seeding technique are needed to improve the flow resolution and resolve small scale vorticity. Despite these differences, the results from this first attempt at imaging flow fields in the air and water agree well with Hendrickson's numerical results. Further tests are warranted to improve PIV resolution on both the air and water side of the wave interface.

The authors would like to acknowledge the financial support of the ONR Young Investigators Program (Award number N00014-04-1-0609) through Dr. Patrick Purtell and Dr. Susan Brown for her consultation on the surface tension measurements.

5 References

Adrian R (2005) Twenty years of particle image velocimetry. *Exp. Fluids*. Online First, 6 July 2005.

Bonmarin P (1989) Geometric properties of deep-water breaking waves. *J. Fluid Mech.*209:405-433.

Chen G; Kharif C (1999) Two-dimensional Navier-Stokes simulation of breaking waves. *Phys. Fluids*. 11(1): 121-133.

Dabiri D; Gharib M (1997) Experimental investigation of the vorticity generation within a spilling water wave. *J. Fluid Mech*. 330: 113-139.

Dommermuth DG; Yue DKP; Lin WM; Rapp RJ; Chang ES; Melville WK (1988) Deep-water plunging breakers: a comparison between potential theory and experiments. *J. Fluid Mech*. 189:423-442.

Dong RR; Katz J; Huang TT (1997) On the structure of bow waves on a ship model. *J. Fluid Mech.* 346:77-115.

Duncan JH (1981) An experimental investigation of breaking waves produced by a towed hydrofoil. *Proc. R. Soc. London Ser. A*. 377:331-348.

Duncan JH (2001) Spilling Breakers. *Annu. Rev. Fluid Mech*. 33:519-547.

Duncan JH; Liu X (2003) The effects of surfactants on spilling breaking waves. *Nature.* 421: 520-523.

Grue J; Liu PLF; Pedersen GK (2004) *Advances in Coastal and Ocean Engineering: PIV and Water Waves* World Scientific Publishing Co. v.9.

Hendrickson KL (2005) Navier-Stokes Simulation of Steep Breaking Water Waves with a Coupled Air-Water Interface. *PhD Thesis*, MIT/Ocean Engineering.

Iafrati A; Di Mascio A; Campana EF (2001) A level set technique applied to unsteady free surface flows. *Inter. J. Numer. Methods Fluids.* 35:281-297.

Kittle PA (2002) Removing foam particles with a foam medium. A2C2 Magazine: Contamination Control for Life Sciences and Microelectronics. January.

Kompenhans J, et al. (1998) *Particle Image Velocimetry:* A Practical Guide. Germany.

McDonald AK (2005) Experimental Investigation of Small-Scale Breaking Waves: Flow Visualization across the Air-Water Interface *MIT Masters Thesis.*

Melville WK (1996) The Role of Surface-Wave Breaking in Air-Sea Interaction. *Ann. Rev. Fluid Mech.* 28: 279:321.

Melville WK; Veron F; White CJ (2002) The velocity filed under breaking waves: coherent structures and turbulence. *J. Fluid Mechanics*. 454: 203-233.

Peirson WL (1997) Measurement of surface velocities and shears at a wavy air-water interface using particle image velocimetry. *Experiments in Fluids.* 23:427-437.

Peregrine DH (1983) Breaking Waves on Beaches. *Ann. Rev. Fluid Mech.* 15:149-178.

Perlin M; He J; Bernal L (1996) An Experimental Study of Deep Water Plunging Breakers. *Phys. Fluids*. 8 (9) 2365-2374.

Rapp RJ; Melville WK (1990) Laboratory Measurements of Deep-Water Breaking Waves. *Phil. Trans. R. Soc. Lond*. A 331: 735-800.

Stanislas M; Okamoto K; Kähler CJ; Westerweel J (2005) Main Results of the Second International PIV Challenge *Exp. Fluids.* Online First, 8 March 2005.

Tsai CP; Chen HB; Hwung HH; Huang MJ (2005) Examination of empirical formulas for shoaling and breaking on steep slopes. *Ocean Engineering.* 32: 469-483.